18èmes Journées Internationales de Thermique (JITH 2017)
Monastir (Tunisie), 25 - 27 Octobre 2017

Double-diffusive natural convection in an inclined rectangular enclosure with heat generation/absorption: Hybrid LBM-FD simulations

Safae Hasnaoui[a,c]*, A. Amahmid[a]*, A. Raji[b], H. Beji[c], M. Hasnaoui[a], Y. Dahani[a] and H. Benhamed[c]

[a]Cadi Ayyad University, Faculty of Sciences Semlalia, LMFE, BP 2390, Marrakech, Morocco
[b]Sultan Moulay Slimane University, Faculty of Sciences and Technics, Physics Department, Laboratory of Flows and
Transfers Modelling (LAMET), B.P. 523, Béni-Mellal 23000, Morocco
[c]Laboratoire des Technologies Innovantes, EA 3899, Université de Picardie Jules Verne, Avenue des Facultés, 80025 Amiens, France

safae.hasnaoui@edu.uca.ac.ma, *amahmid@uca.ac.ma, abderaji@yahoo.fr, hassen.beji@u-picardie.fr, hasnaoui@uca.ac.ma, youssef.dahani@taalim.ma and haykel.benhamed@u-picardie.fr*

Abstract: We study numerically the impact of the inclination angle of a rectangular cavity on thermosolutal natural convection in the presence of Soret effect and heat generation. The enclosure is differentially heated and salted from two opposite long sides with constant but different temperatures and concentrations while the short walls are considered adiabatic and impermeable to mass transfer. A hybrid lattice Boltzmann-finite difference method (LBM-FD) is used to analyze the effect of the governing parameters and the results are presented in terms of streamlines, isotherms, iso-concentration lines, mean temperatures and concentrations and local and averaged Nusselt and Sherwood numbers on the active walls. The governing parameters of this problem are the external Rayleigh number($Ra_E = 10^5$), the Prandtl number ($Pr = 0.71$), the buoyancy ratio ($N = 1$), the Lewis number ($Le = 2$), the Soret parameter ($Sr = 0$ and -0.5), the internal to external Rayleigh numbers ratio $0 \leq R \leq 80$ and the cavity inclination γ , varied from 0° (vertical position) to 60°.

Keywords: Heat transfer, Thermodiffusion natural convection, heat generation/absorption, Hybrid LB-FD method.

1. Introduction

Problems involving heat and mass transfer by free convection in rectangular cavities including both fluid and porous media has attracted considerable attention through the decades owing to their practical implications in many engineering and environmental requests. The combined effects of thermal and solutal buoyancy forces lead to more complex flow structures in comparison with the pure thermal convection. The consideration of cross diffusion (i.e. Soret and/or Dufour effects) in recent problems further complicate the nature of the coupling resulting in very specific behaviors. In the case of cavities differentially heated and salted, the fluid flow is, in general, easily triggered (except in special cases as in situations where thermal and buoyancy forces are opposing to each other) in the medium by imposing horizontally a gradient of temperature and/or a gradient of concentration. These kinds of problems have been considered in many experimental and numerical studies [1-7]. Sometimes, these gradients should exceed some critical thresholds to trigger convection flows when thermal and solutal gradients are parallel to gravity [8-11]. Such a category of problems lead in general to more intriguing solutions which are (but not limited to) oscillatory flows, Hopf bifurcations, hysteresis behaviors and reversal gradients of concentration. In some practical situations, when the separation of species is a researched goal, the inclination of the cavity could help by attenuating velocity flows to amounts ensuring optimum conditions that lead to maximum separation of the species [12-15]. The important role that may be played by this parameter (inclination) in the modification of buoyancy forces has been demonstrated in the case of thermal convection induced in a square cavity; its effect was examined on the melting rate [16] and on heat transfer in the presence of nanoparticles [17-19]. Another phenomenon, which is expected to alter heat and mass transfer characteristics in rectangular cavities, is the internal heat generation. The latter has been the object of experimental [20, 21] and numerical [22, 23] studies dealing with thermal natural convection. Comparatively, literature shows that very limited research has been conducted on thermosolutal natural convection for an internally heated cavity [24]. The impact of the heat generation is measured by properly defining an internal Rayleigh number, Ra_I, while the flow generated by the temperature and concentration differences is attributed to an external Rayleigh number, Ra_E. The ratio Ra_I/Ra_E may play a key role in the control of fluid flow and heat and mass transfer characteristics. Thus, having regard to the existing, the present study is dedicated to investigate thermosolutal natural convection in an inclined rectangular cavity with an aspect ratio of 2 by focusing the attention on the combined effects of the cavity inclination and the ratio of internal and external Rayleigh numbers. The numerical code, based on the hybrid FD-LBM method, was successfully validated with a homemade code based on the lattice-Boltzmann method, with the multi-relaxation time (MRT) scheme.

2. Mathematical Formulation

2.1 Problem Description

The physical model considered in the present study is sketched in Fig. 1. It is a 2D rectangular cavity of height, H and width, L confining a binary mixture. The long sides of the enclosure, parallel to Oy, are submitted to constant temperatures ($T_0 < T_1$) and concentration ($S_0 < S_1$) while its short sides are considered adiabatic and impermeable to mass transfer. The confined mixture is considered Newtonian, incompressible, obeying the Boussinesq approximation and the fluid flow is laminar. By considering these hypotheses, the macroscopic governing non-dimensional equations have been obtained by using appropriate dimensionless variables. In the vorticity-stream function formulation, ($\Omega - \psi$), and in the presence of Soret effect, these equations can be presented as follows:

$$\frac{1}{Pr}\left[\frac{\partial\Omega}{\partial t}+\frac{\partial(u\Omega)}{\partial x}+v\frac{\partial(v\Omega)}{\partial y}\right]=\nabla^2\Omega+R_{aE}\left[\left(\frac{\partial\theta}{\partial x}+N\frac{\partial\phi}{\partial x}\right)\cos(\gamma)-\left(\frac{\partial\theta}{\partial y}+N\frac{\partial\phi}{\partial y}\right)\sin(\gamma)\right] \quad (1)$$

$$\frac{\partial\theta}{\partial t}+\frac{\partial(u\theta)}{\partial x}+\frac{\partial(v\theta)}{\partial y}=\nabla^2\theta+R \quad (2)$$

$$\frac{\partial\phi}{\partial t}+\frac{\partial(u\phi)}{\partial x}+\frac{\partial(v\phi)}{\partial y}=\frac{1}{Le}(\nabla^2\phi+Sr\nabla^2\theta) \quad (3)$$

And

$$\frac{\partial^2\psi}{\partial x^2}+\frac{\partial^2\psi}{\partial y^2}=-\Omega \quad (4)$$

The local Nusselt and Sherwood numbers are evaluated as:

$$Nu_{1,0}(y)=-\left.\frac{\partial\theta}{\partial x}\right|_{x=0,1} \text{ and } Sh_{1,0}(y)=-\left(\left.\frac{\partial\phi}{\partial x}\right|_{x=0,1}+Sr\left.\frac{\partial\theta}{\partial x}\right|_{x=0,1}\right) \quad (5)$$

In the above equation, the subscript 0/1 of Nu and Sh stays for the heated/cooled wall.

The averaged Nusselt and Sherwood numbers on the active walls are defined as follows:

$$Nu_{1,0}=-\frac{1}{H}\int_0^H\left.\frac{\partial\theta}{\partial x}\right|_{x=0,1}dy \text{ and } Sh_{1,0}=-\frac{1}{H}\int_0^H\left(\frac{\partial\phi}{\partial x}+Sr\left.\frac{\partial\theta}{\partial x}\right|_{x=0,1}\right)dy \quad (6)$$

The examination of the governing equations, written in their dimensionless form, shows that the control parameters are $S_r=\frac{D_{CT}\Delta T}{D\Delta S}$; the Soret parameter, $\theta/(\phi)$; the dimensionless temperature/(concentration), $Le=\frac{\alpha}{D}$; the Lewis number, $Pr=\frac{\nu}{\alpha}$; the Prandtl number, $N=\beta_S\Delta S/(\beta_T\Delta T)$; the buoyancy ratio, γ; the cavity inclination and $R=\frac{Ra_I}{Ra_E}$; internal to external Rayleigh numbers ratio, with $Ra_E=g\beta\Delta TL^3/(\upsilon\alpha)$ and $Ra_I=g\beta\dot{Q}L^5/(\upsilon\alpha\lambda)$. These two last parameters are respectively controlled by the temperature difference between the active boundaries and the intensity of the uniform volumetric heat generation/absorption rate. It is to specify that the presentation of the dimensionless Eqs. (1) to (4) in this manuscript was motivated by the concern to make explicitly appearing the governing parameters.

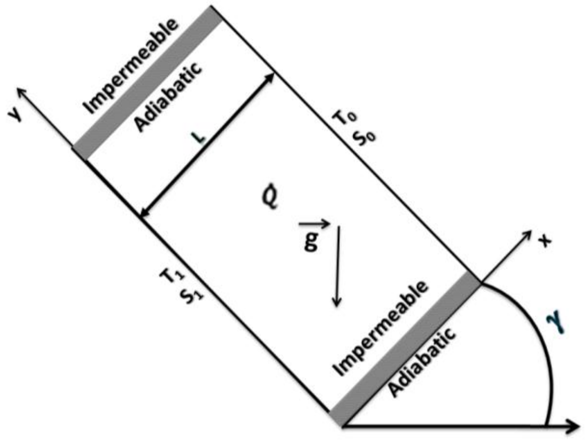

Figure 1. Physical model

2.2 Mathematical formulation

In the mesoscopic approach used in this study, the problem is governed by the Boltzmann equations (6) for the momentum equation using the Bhatnagar–Gross–Krook (BGK) approximation [25] while the equations of advection-diffusion of temperature and concentration are solved separately using an explicit finite-difference technique at the Boltzmann scale. The Lattice-Boltzmann equation in the presence of an external force F can be written for the flow field as follows:

$$f_k(r + c_k\Delta t, t + \Delta t) = f_k(r,t) - \omega_v.\left(f_k(r,t) - f_k^{eq}(r,t)\right) + F_k\Delta t \qquad (6)$$

In the precedent equation, $\omega_v = 1/\tau_v$ stays for the flow field collision frequency. The parameters τ_v and Δt represent the flow relaxation time and the linkage time, respectively. To treat the incompressible case, we used the model proposed by He and Luo [26] who suggested to neglect the terms of order higher than 2 in terms of the Mach number.

Thereby the local equilibrium distribution function, $\mathrm{f_k^{eq}}(\mathrm{r,t})$, known also as Maxwell's distribution function, is obtained as [27]:

$$f_k^{eq}(r,t) = \omega_k\rho\left[1 + 3\frac{\vec{c}_k.\vec{u}}{c^2} + 4.5\frac{(\vec{c}_k.\vec{u})^2}{c^4} - 1.5\frac{\vec{u}.\vec{u}}{c^2}\right] \quad \text{for k = 0, 1, …, 8} \qquad (7)$$

With ρ being the density, $\vec{\mathrm{c}}_\mathrm{k}$ the discrete velocities for the arrangement D2Q9 scheme (used in this study), ω_k the weighting factor and c the lattice speed. The implementation of the Boussinesq approximation in the discrete external force was derived from the expression proposed by Luo [28] as follows:

$$\mathrm{F_k} = 3\omega_\mathrm{k}\mathrm{F} = 3\omega_\mathrm{K}\rho g\beta((\mathrm{T} - \mathrm{T_m}) + \mathrm{N}(\mathrm{S} - \mathrm{S_m}))\left(\mathrm{c_{ky}}\cos\gamma + \mathrm{c_{kx}}\sin\gamma\right) \qquad (8)$$

Where $\mathrm{T_m} = (\mathrm{T_1} + \mathrm{T_0})/2$, $\mathrm{S_m} = (\mathrm{S_1} + \mathrm{S_0})/2$, β is the thermal expansion coefficient and $\mathrm{c_{kx}}$ and $\mathrm{c_{ky}}$ are the projections of the microscopic velocity $\vec{\mathrm{c}}_\mathrm{k}$ on the x and y axes.

The macroscopic quantities which are the density, ρ, and the velocity, $\vec{\mathrm{u}}$, can be obtained by using the following formulas:

$$\begin{cases} \rho(\mathrm{r,t}) = \sum_{\mathrm{k=0}}^{\mathrm{k=8}} \mathrm{f_k}(\mathrm{r,t}) \\ \rho\vec{\mathrm{u}}(\mathrm{r,t}) = \sum_{\mathrm{k=0}}^{\mathrm{k=8}} \vec{\mathrm{c}}_\mathrm{k}\mathrm{f_k}(\mathrm{r,t}) \end{cases} \qquad (9)$$

The Chapman-Enskog procedure [29] was used to link the kinematic viscosity ν to the relaxation time as $\nu = (\tau_V - 0.5)\frac{c^2}{3}\,\Delta t$.

As mentioned before, the energy and species equations are written in their dimensional forms as follows:

$$\frac{\partial T}{\partial t} = u\frac{\partial T}{\partial x} + v\frac{\partial T}{\partial y} = \alpha\left(\frac{\partial^2 T}{\partial x^2} + \frac{\partial^2 T}{\partial y^2}\right) + \frac{\dot{Q}}{\varrho Cp} \quad (10)$$

$$\frac{\partial S}{\partial t} = u\frac{\partial S}{\partial x} + v\frac{\partial S}{\partial y} = \varkappa_{21}\left(\frac{\partial^2 T}{\partial x^2} + \frac{\partial^2 T}{\partial y^2}\right) + D\left(\frac{\partial^2 S}{\partial x^2} + \frac{\partial^2 S}{\partial y^2}\right) \quad (11)$$

Where α and D stay respectively for thermal and mass diffusivities while the parameter $\varkappa_{21}$ translates the coupling due to the Soret effect. Equations (10) and (11) were discretized at the Boltzmann scale using a similar approach to that proposed by Lallemand and Luo [30] with $\Delta t = \Delta x = \Delta y = 1$. This method is explicit and characterized by a conditional convergence criterion. The object in the present study was to extend its use to the present problem. More specifically, for Eqs. (10) and (11), the following discretizations were used:

$$\frac{\partial \Gamma}{\partial t} = \Gamma_{i,j}^{n+1} - \Gamma_{i,j}^{n} \quad (12)$$

$$\frac{\partial \Gamma}{\partial x} = \Gamma_{i+1,j}^{n} - \Gamma_{i-1,j}^{n} - \frac{1}{4}\left(\Gamma_{i+1,j+1}^{n} - \Gamma_{i-1,j+1}^{n} + \Gamma_{i+1,j-1}^{n} - \Gamma_{i-1,j-1}^{n}\right) \quad (13)$$

$$\frac{\partial^2 \Gamma}{\partial x^2} + \frac{\partial^2 \Gamma}{\partial y^2} = 2\left(\Gamma_{i+1,j}^{n} + \Gamma_{i-1,j}^{n} + \Gamma_{i,j+1}^{n} + \Gamma_{i,j-1}^{n}\right) - \frac{1}{2}\left(\Gamma_{i+1,j+1}^{n} + \Gamma_{i-1,j+1}^{n} + \Gamma_{i+1,j-1}^{n} + \Gamma_{i-1,j-1}^{n}\right) \quad (14)$$

In Eqs. (12) to (14), Γ stays for T or S and the first derivative of Γ with respect to y is similar to its derivative with respect to x in Eq. (13), if one takes care to permute the roles of the indices “i” and “j”. The parameters α and D where calculated at the Boltzmann scale as $\alpha = \nu/Pr$ and $D = \alpha/Le$ while the source term in Eq. (10) was calculated by using the available data.

2.2 Validation of the numerical code

The hybrid LBM-FD code was validated against a homemade code based on LBM with MRT scheme, developed by our team, and using D2Q9 model for fluid flow and D2Q5 models for temperature and concentration. Various comparative tests have been successfully carried out but illustrated here just for the case $N = 1$, $Ra = 10^5$, $Le = 2$, $R = 40$, $A = 2$ and $\gamma = 45°$. Comparisons were made in terms of streamlines, isotherms, iso-concentrations and corresponding extremum values of ψ and mean values of Nusselt and Sherwood numbers on the active boundaries. The comparative results presented in Fig. 2 were obtained with a grid 120×240 (the same grid used in this study). The examination of these results show an excellent qualitative agreement between both methods. Despite the difference in the approaches used for both methods, only a maximum relative difference of about 3.4%/1.9% is observed in terms of ψ_{max}/ψ_{min} while for Nusselt and Sherwood numbers, the maximum difference remains within 0.6%.

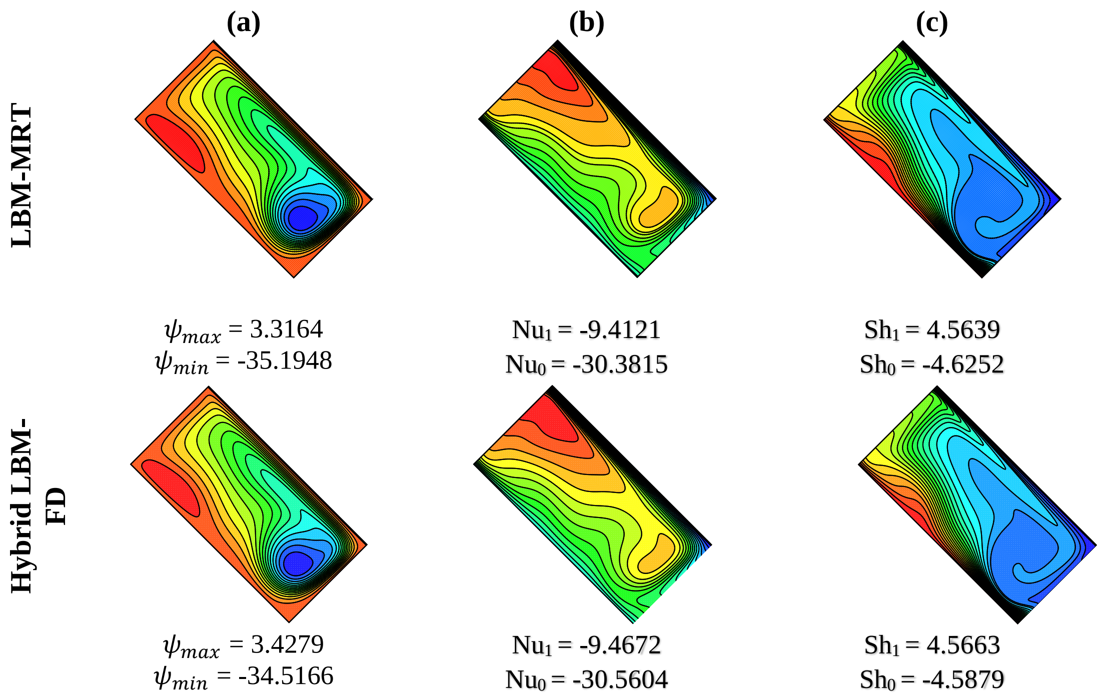

Figure 2: Validation of the numerical code in terms of streamlines (a), isotherms (b) and iso-concentrations (c) for $Sr = 0$, $\boldsymbol{N} = 1$, $Ra = 10^5$, $Le = 2$, $R = 40$, $A = 2$ and $\gamma = 45°$.

2.3 Effect of the grid

The preliminary tests conducted to examine the sensitivity of the results vis-à-vis of the grid has led to the choice of the grid 120×240 for the present study. The comparative indicative results presented in Table 1 provide an idea about the changes accompanying the refinement of the grid. It can be affirmed that the selected grid (120×240) leads to very satisfactory results compared with the finer grid (160×320) with an important gain in computation time. Quantitatively, the results engendered by choosing the grid 120×240 deviate by less than 0.43% from those obtained with the finest grid.

Table 1 : Grid's effect for $Sr = 0$, $\boldsymbol{N} = 1$, $Ra = 10^5$, $Le = 2$, $R = 100$, $A = 2$ and $\gamma = 45°$.

	$\boldsymbol{\psi_{max}}$	$\boldsymbol{\psi_{min}}$	Nu_1	Nu_0	Sh_1	Sh_0
80×160	10.9099	-38.8955	-30.6780	-69.9169	3.7887	-3.8377
100×200	10.9689	-38.8697	-30.6485	-69.6767	3.7751	-3.8040
120×240	11.0031	-38.8761	-30.6381	-69.5554	3.7689	-3.7869
140×280	11.0277	-38.8843	-30.6345	-69.4884	3.7658	-3.7777
160×320	11.0498	-38.8895	-30.6337	-69.4486	3.7642	-3.7724
Relative deviation (%)	0.4226	0.0345	0.0144	0.1538	0.1249	0.3844

3. Results and discussion

The results presented in this section were obtained with the hybrid lattice-Boltzmann finite-difference method in the case of a cavity heated and salted from the long opposite sides for $N = 1$ (case of aiding buoyancy forces). The remaining parameters are the aspect ratio of the cavity ($A = 2$), the Lewis number ($Le = 2$), the Prandtl number ($Pr = 0.71$), the external Rayleigh number ($Ra_E = 10^5$), the cavity inclination ($\gamma = 0°$, $30°$ and $60°$), the Soret parameter ($Sr = 0$ and -0.5) and the parameter R characterizing the relative importance of the internal Rayleigh number compared to that of the external Rayleigh number ($0 \leq R \leq 80$). The restricted choice of the values of the control parameters was dictated by the concern to avoid unsteady solutions more frequently observed for positive values of Sr (particularly for $Sr = 0.5$ considered in the preliminary tests), which requires more investigative effort that goes beyond a scope of a conference. In addition, the case of heat absorption was omitted since their corresponding results may be deduced from the case of heat generation as indicated in Fig. 3 for two opposite values of R. Here, we illustrate combined effects of the three parameters which are Sr, R and γ on the illustrative results presented hereafter.

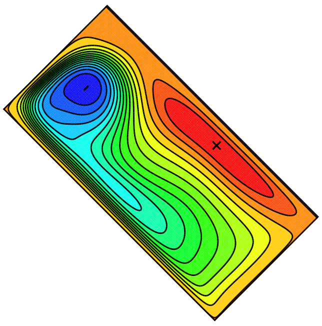

(a)

$(\psi_{max}, \psi_{min}) = (8.563, -37.617)$
$(Nu_1, Nu_0) = (56.589, 23.534)$
$(Sh_1, Sh_0) = (3.705, -3.684)$

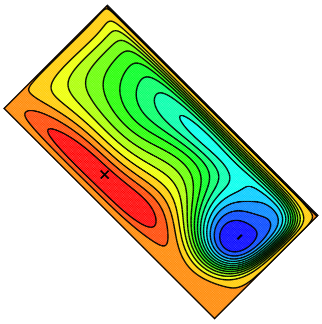

(b)

$(\psi_{max}, \psi_{min}) = (8.563, -37.617)$
$(Nu_1, Nu_0) = (-23.534, -56.589)$
$(Sh_1, Sh_0) = (3.684, -3.705)$

Figure 3: Streamlines for $\mathrm{N} = 1$, $\mathrm{Sr} = 0$, $Ra = 10^5$ and $\gamma = 45°$: (a) $R = -80$ and (b) $R = 80$.

3.1 Fluid flow and heat and mass transfer characteristics

The combined effects of cavity inclination and Soret parameters are depicted in Figs. 4a-b for $R = 0$ and Figs. 4c-d for $R = 80$ in the absence of Soret effect (Figs. 4a and 4c) and in the presence of negative Soret effect (Figs. 4b and 4d). It can be seen that the flow circulation is mainly structured in one negative clockwise rotating cell. It is however to outline that the solution obtained with $Sr = -0.5$ and $\gamma = 60°$ is unsteady periodic but the flow doesn't lose the monocellular structure (the quantitative results presented for this case correspond to average quantities over one flow cycle). For this unsteady solution, only slight qualitative changes affecting the internal lines of the cell were observed. As for the flow intensity, it undergoes nevertheless an important change around 37% during the evolution of the flow cycle. Apart from this clarification, all the remaining solutions are steady. Globally, by focusing the attention on the Soret effect for a given inclination, we notice that the negative Soret parameter has a negative impact on the flow intensity. More specifically, for $\gamma = 60°$, the flow intensity undergoes a mean decrease around 8.4% by changing the value of Sr from 0 to -0.5. Comparatively, the decrease registered is around 13%/10.5% for $\gamma = 30°/0°$ when the Soret effect is considered. Now, by focusing the attention on the changes undergone by varying the cavity inclination, it appears that these changes are more important. Qualitatively, the variation of the parameter γ engenders a big change in the shape of the internal lines of the cells; changes visibly more marked by the inclination variations that affect the components of the buoyancy force. Quantitatively, for a given Soret parameter, by decreasing the cavity inclination from 60° to 30°/0°, the flow intensity decreases by about 31%/47% for $Sr = 0$ and 34%/48% for $Sr = -0.5$. It is to note that the increase of the ratio R of the Rayleigh numbers destroys the monocellular flow structure by favoring the appearance of a positive small cell from a critical value of R that depends both on γ and Sr. The figure 2 used for a validation purpose gives an idea about the size and location of the nascent positive cell for the corresponding combinations of the governing parameters. For $R = 80$, Figs. 4c and 4d exemplify other states of the flow respectively for $Sr = 0$ and -0.5 and various γ. It is seen that this relatively important value of R has led to a big change in the flow structure by favoring the positive clockwise cell in terms of size and intensity. The latter appears when the hot wall contributes to the cooling process (i.e its role changes to ensure the evacuation of a part of the important heat generated inside the cavity). Another point to outline is the fact that all the solutions obtained with $R = 80$ are steady. Recall that for $R = 0$ the flow structure is monocellular. For R = 80, the monocellular nature of the flow is lost, which means that the size of the negative cell is reduced but, despite this fact, its intensity is increased since it is supported by the internal heat generation. More specifically, the increase of the flow intensity accompanying the increase of R for $Sr = 0/-0.5$ is of about 32%/21%, 79%/68% and 98.5%/79.5%, respectively for $\gamma = 60°$, 30° and 0°. Now, by focusing the attention on the relative ratio (in %) of the positive cell's intensity with respect to that of the negative one for each inclination, we notice that it is of about 16.2%, 30.6% and 48.3%, respectively for $\gamma = 60°$, 30° and 0° and $Sr = 0$. However, for $Sr = -0.5$, these ratios become respectively 19.5%, 32.9% and 48.8%. This means that the decrease of the cavity inclination attenuates both the positive and negative cells intensities and these relative attenuations are more important for the considered negative value of the Soret parameter.

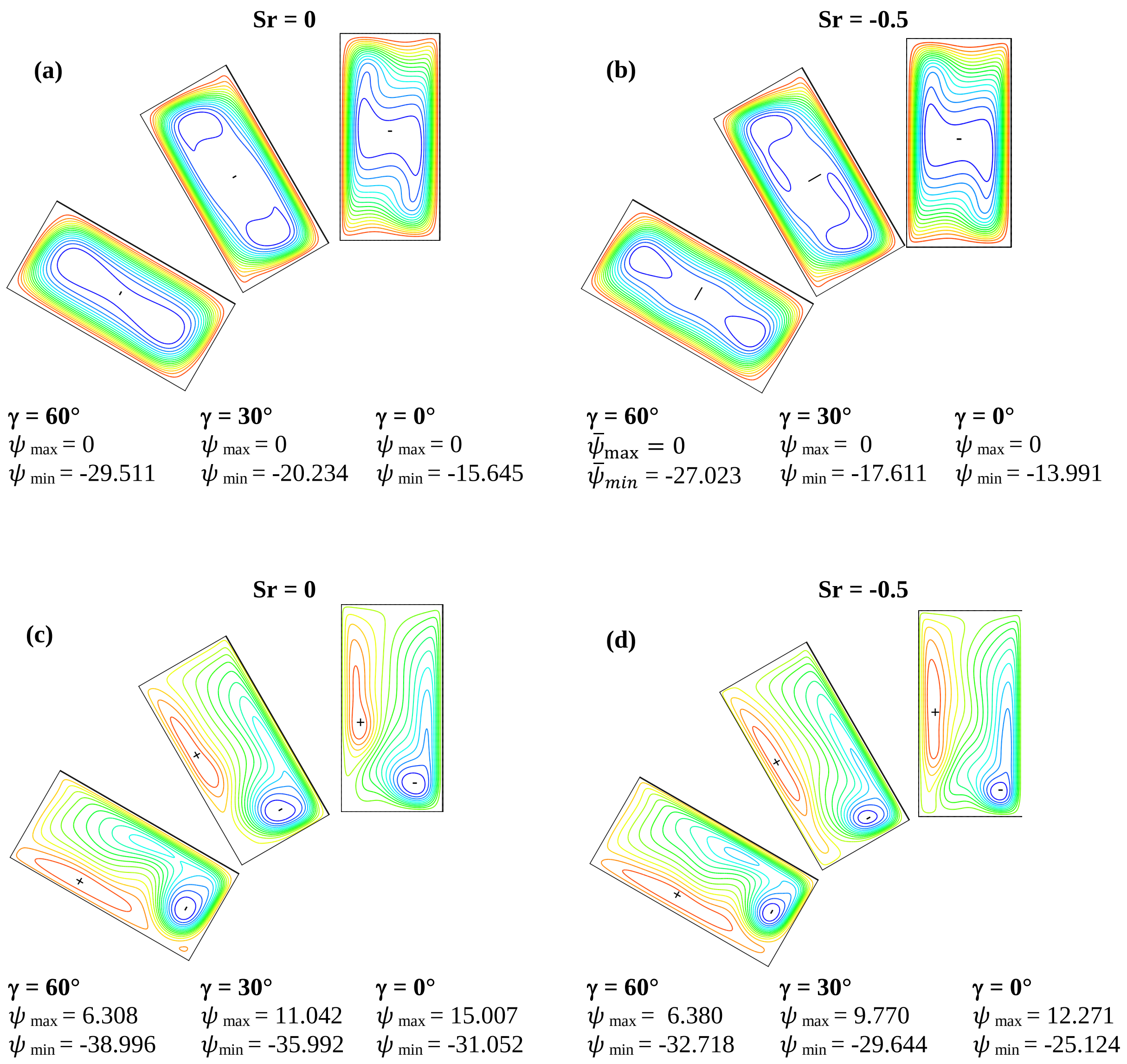

Figure 4: Streamlines for $\mathrm{Sr} = 0$ (a, c) and -0.5 (b, d), $\mathrm{R} = 0$ (a, b) and 80 (c, d), $Ra = 10^5$ and various γ.

The corresponding isotherms are illustrated in Figs. 5a-b for $R = 0$ and in Figs. 5c-d for $R = 80$ in the absence (Figs. 5a and 5c) and in the presence (Figs. 4b and 4d) of Soret effect. These figures show that the isotherm fields are affected by the Soret parameter and more importantly by the inclination of the cavity. In the absence of heat generation ($R = 0$), the mean heat fluxes crossing the active boundaries are identical in the absence and in the presence of Soret effect indicating that the energy balance is fully satisfied. For $R = 80$, the sum (in absolute value) of both Nusselt numbers should be equal 80. This balance is also satisfied with a maximum error of 0.4%. Moreover, in the absence of internal heat generation and, due to the monocellular nature of the flow, two thermal boundary layers are developed in the upper part of the cooled wall and in the lower part of the heated one. The locations of these boundary layers can be explained by the clockwise rotation of the unique existing cell. In fact, these boundary layers are observed there where the fluid heated/cooled by the left/right wall interacts first with the cooled/heated wall. For $R = 80$, the most important temperature gradients are still located on the upper part of the cold wall but on the heated wall, they are shifted towards its upper part, where the peripheral lines of the positive counter-clockwise rotating cell, generated by the internal heating, comes in contact with the heated wall. In fact, the imposed temperature of the heated wall becomes lower than that of the confined fluid for the considered value of R and the most temperature difference between the fluid and the heated wall is observed in its upper part and decreases along the heated wall toward the bottom of the cavity with the downward movement of the peripheral lines. In addition, the internal heat generation destroys the thermal stratification observed in the central part of the cavity for $\gamma = 30°$ and 0° owing to the new structure favored by the internal heat generation. For $R = 80$, 40.2% of heat is evacuated from the heated wall for $\gamma = 60°$. This relative ratio becomes 44.9% and 60.6% for $\gamma = 30°$ and 0°, respectively. These differences indicate the important role played by the inclination of the cavity in the control of the quantity of heat evacuated through the active boundaries.

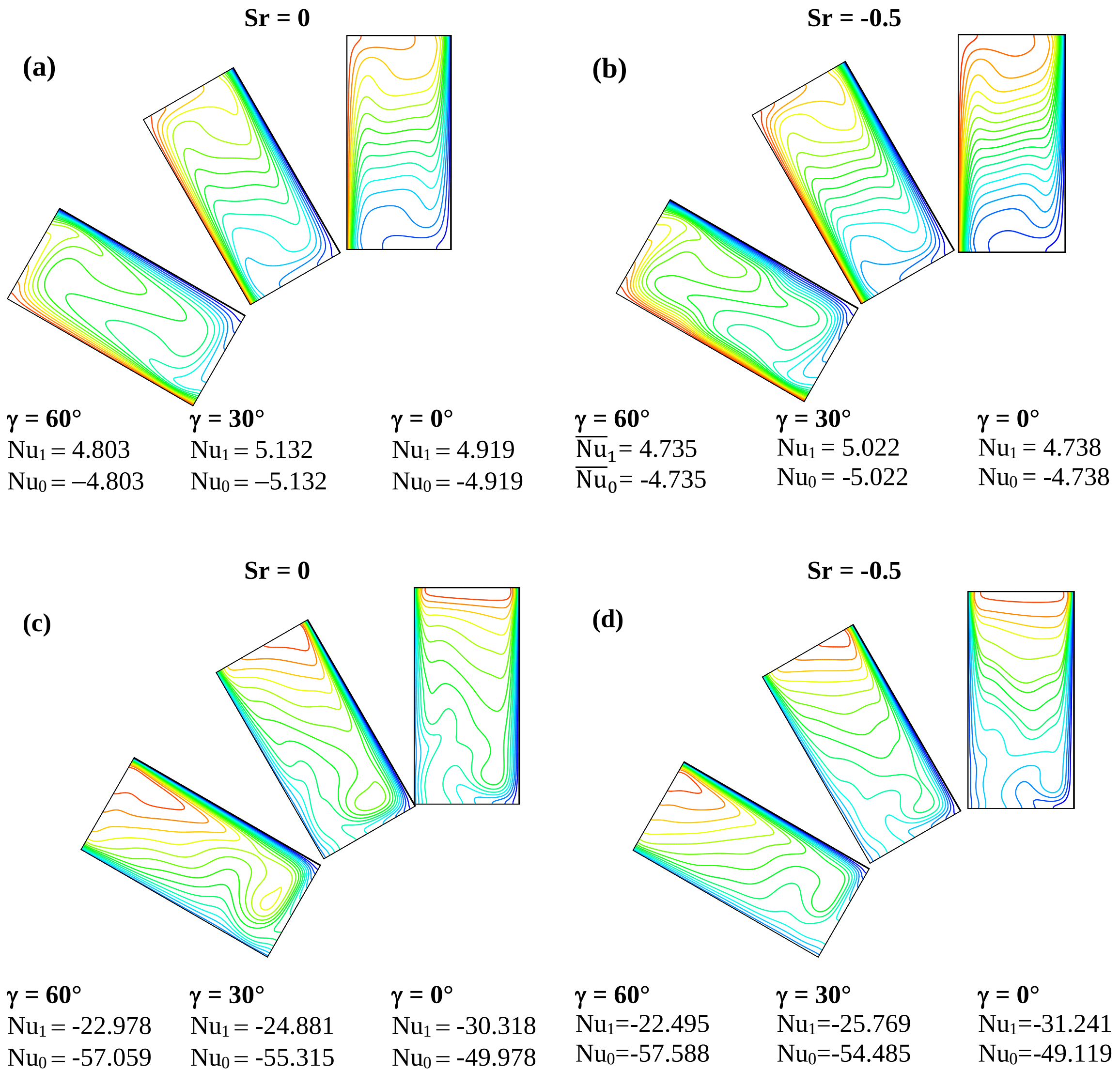

Figure 5: Isotherms for $\mathrm{Sr} = 0$ (a, c) and -0.5 (b, d), $R = 0$ (a, b) and 80 (c, d), $Ra = 10^5$ and various γ.

The iso-concentration lines exemplified in Figs. 6a-b for $R = 0$ and in Figs. 6c-d for $R = 80$ in the absence (Figs. 6a and 6c) and in the presence (Figs. 6b and 6d) of Soret effect, are seen to be qualitatively more sensitive than the isotherms to the variations of the governing parameters. Similarly to the temperature field, the most important concentration gradients are observed on the upper/lower part of the less/most salted wall due the unicellular nature of the flow and its clockwise rotation for $R = 0$. The mean Sherwood numbers are also identical on both salted boundaries in the absence of internal heat generation but a maximum relative difference of about 6.8% is observed between Sh_1 and Sh_0 for $R = 80$ without any change in the direction of the concentration gradients on the active boundaries. Quantitatively, the Sherwood numbers are weaker in the presence of Soret effect. More specifically, for $R = 0$, the increment of Sr from 0 to -0.5 leads to a decrease of Sherwood number of about 23.6%, 27.3% and 23.1% for $\gamma = 60°$, 30° and 0°, respectively. For the same value of R, and in the absence of the Soret effect, the Sherwood number varies slightly (it undergoes a slight increase of about 7.7%) when the cavity inclination varies from 60° to 0°. This increase goes to about 8.4% for $Sr = -0.5$. In addition, for $R = 80$, the Sherwood number drops seriously in comparison with $R = 0$ for given Sr and γ and the field of concentration is visibly more affected by the existence of the positive cell than the temperature field. In fact, it can be seen that important gradients of concentration, normal to the long sides of the cavity, are present in the area between the ascending lines at the interface of the two cells for $Sr = 0$ and also the area of high concentrations, generated for the negative Soret parameter are more affected by the inclination of the cavity.

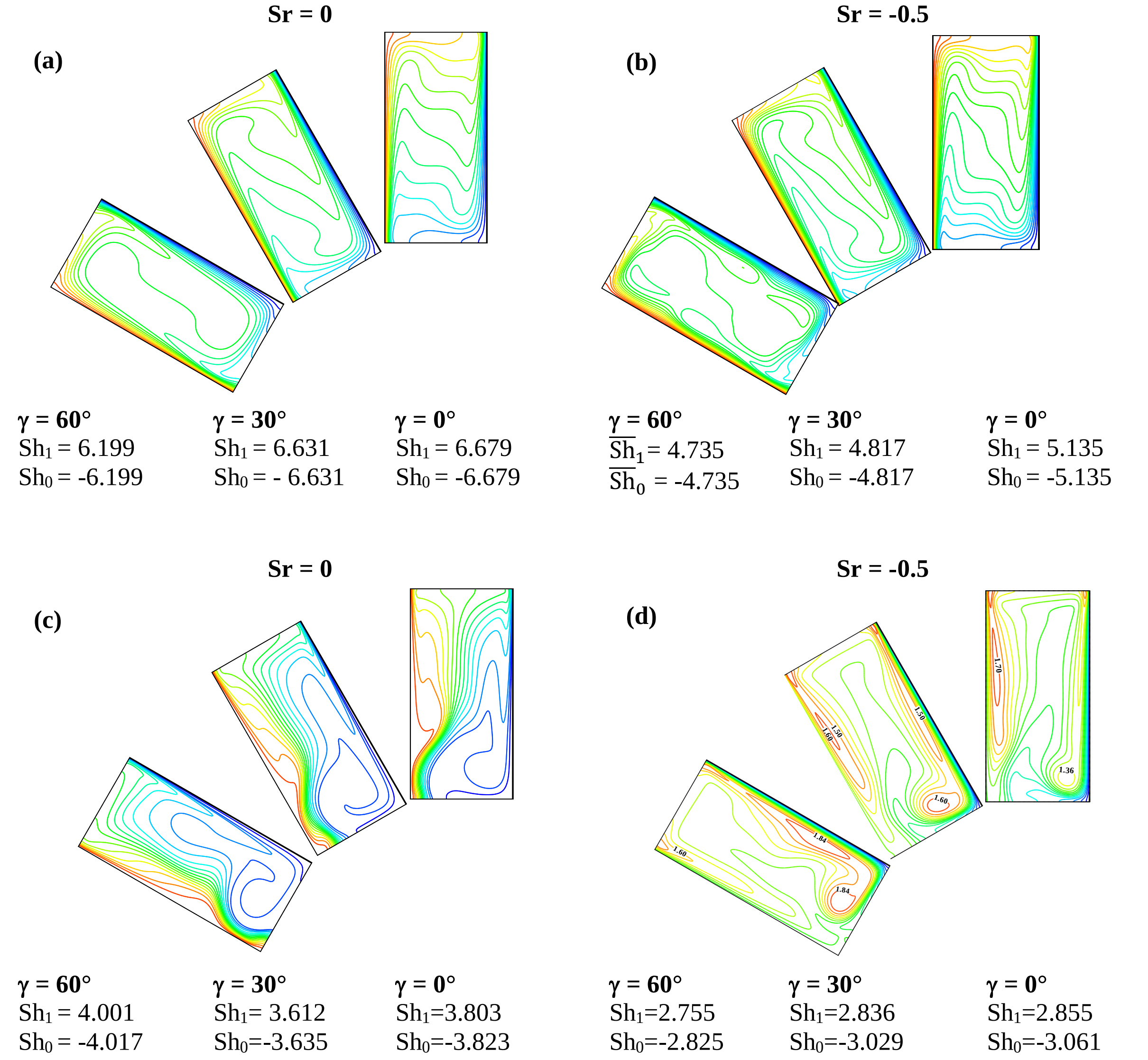

Figure 6: Iso-concentrations for $\mathrm{Sr} = 0$ (a, c) and -0.5 (b, d), $\mathrm{R} = 0$ (a, b) and 80 (c, d), $Ra = 10^5$ and various γ.

3.1 *Mean temperature and concentration*

The mean temperature variations vs. R, illustrated in Fig.7a, are characterized (as expected) by an increase with the internal heating rate regardless of the inclination and the Soret parameter. In some range of R (say above 20), a quasi-linear variation is observed with a slope that increases with the inclination. The effect of the inclination on the mean temperature is more important at high R. Quantitatively, at $R = 80$, the mean temperature obtained for $\gamma = 60°$ is 17.37%/ 13.26% higher than the one obtained with 0° inclination for $Sr = 0$/(-0.5). Hence, the inclination 60°, compared to 30° and 0°, is seen to be the most unfavorable to the cooling process of the cavity. This inclination ($\gamma = 60°$) may be of usefulness only when the objective is to reduce heat losses from the cavity boundaries. Note that the intensity of the secondary positive cell is strongly reduced in the case of $\gamma = 60°$; it is nearly halved/(divided by a factor of 2.4) when the inclination is increased from zero to 60° for Sr = -0.5/0. The latter cell, covering all the hot wall (with a weak intensity), plays a resistant role to the heat evacuation from the heated wall.

Due to thermodiffusion that affects directly the conservation of species, the mean concentration is seen to be strongly dependent on the Soret parameter as exemplified in Fig.7b. Thus, in the absence of Soret effect ($Sr = 0$), the mean concentration is nearly constant over a large range of R ($R \geq 20$) with a value not far from 0.5 (i.e. the value obtained at $R = 0$). For $Sr = -0.5$, we observe an increase of the mean concentration with R. For $\gamma = 60°$, The latter is multiplied by 2.74 when R increases from 0 to 80. In fact, at sufficiently large values of R, the temperature gradient is directed outward on both active walls, so the thermodiffusion creates an inward mass flux on both active walls. This mass flux is intensified by the increase of R (due to the increase of the temperature gradient). The effect of the inclination on the mean concentration is seen to be much more important in the range 30°-60° than in the range 0°-30°. At $R = 80$, for instance, the mean concentration increase by 5.95%/16.85% when γ increases from 0/30° to 30°/60°. These results show that negative Soret parameter combined with high internal heat generation and a relatively high inclination is important when the objective is to charge the fluid with species.

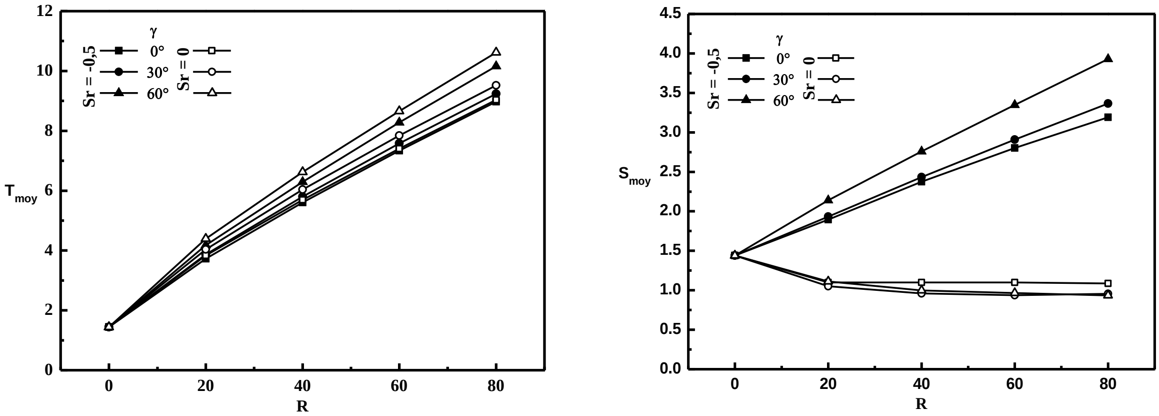

(a) **(b)**

Figure 7: Average Temperature (a) and concentration (b) variations vs. R for various Sr and γ.

3.2 Local heat and mass transfer

Variations of local Nusselt numbers along both active walls are illustrated in the cases of $Sr = 0$ (Figs. 8a-b) and $Sr = -0.5$ (Figs. 8c-d) for $R = 0$ and 80 and various values of γ. For $R = 0$, Fig. 8a shows that the local Nusselt number is positive on the left wall (i.e. the hot wall) and it is generally decreasing along this wall. This behavior is compatible with the monocellular flow obtained for $R = 0$. In fact, the clockwise negative cell brings the coldest currents towards the lower part of hot wall that plays a heating role in the absence of internal heating. Quantitatively, the effect of the inclination on the local heat transfer is important. For $y = 0$/($y = 2$), for instance $Nu_1(y)$ is divided/(multiplied) by 1.69/1.77 when γ increases from 0° to 60°. For $R = 80$, the temperature of the fluid is so high that the sign of $Nu_1(y)$ becomes negative indicating that the hot wall changes its role and becomes forced to contribute to the cooling process due the inversion of the temperature gradients near the heated wall. Also, the most important heat transfer occurs at the upper part of the left wall as the flow becomes bicellular and the ascending hot currents of the positive cell (heated by the internal generation) interacts first with the upper part of the left wall before their downward movements along the latter. The effect of the inclination on the local heat transfer is very remarkable in this case. The local heat transfer is globally favored by the inclination 0° on the heated wall from y ≥ 0.5. However, the important gap exhibited by the curves in the upper part of the heated wall (at y = 2, $Nu_1(y)$ is divided by two when γ increases from 0° to 60°) indicates that, in average, the inclination 60° is manifestly less favorable to heat transfer. On the right wall, the local Nusselt number $Nu_0(y)$ variations, exemplified in Fig. 8b, are similar to those obtained for the left wall in absolute values in the case of $R = 0$ (the negative sign indicates that the right wall plays a cooling role) due to the centro-symmetry of the flow. Because of this centro-symmetry, the upper/lower half of the right wall plays the role of the lower/upper half of the left one. At $R = 80$, the presence of a bicellular non-symmetrical flow leads to a different behavior on the right wall. Particularly, we can see that the inclination 60° overcomes the other inclinations in terms of heat transfer in a large part (for y ≤ 1.5) of the right wall. For this case, the important gap observed between the curves of 0° and 30° in the upper part of the left wall is considerably reduced in the case of the right wall (the curves of $Nu_0(y)$ are nearly coincident in the vicinity of y = 2).

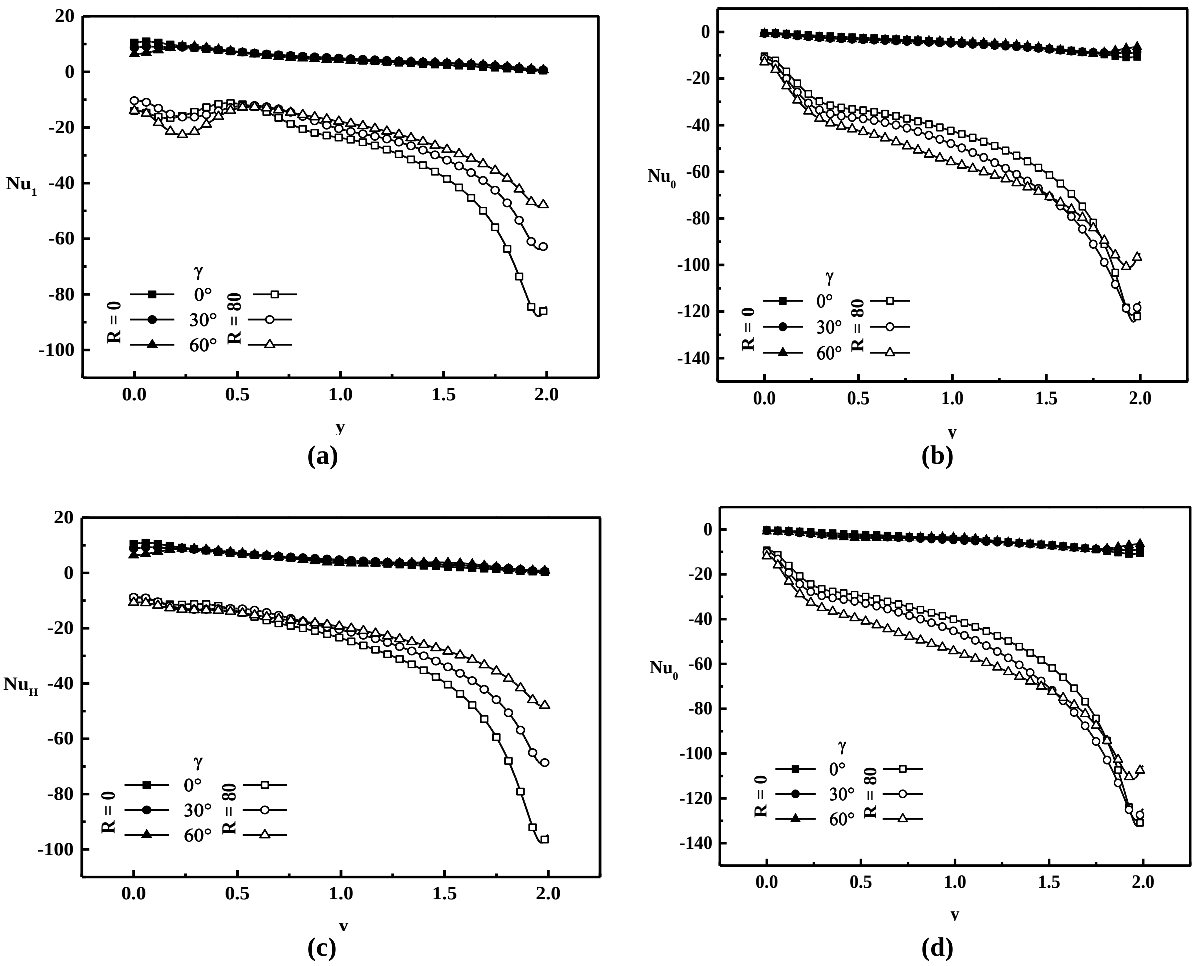

Figure 8: Local Nusselt number in the heated (a, c) and cooled (b, d) walls for; $\mathrm{Sr} = 0$ (a, b) and -0.5 (c, d) and various γ.

The local Sherwood number is exemplified in Fig. 9a-d. For $Sr = 0$, Fig.9a shows the variations of Sh with y on the heated wall. For $R = 0$, Sh_1(y) goes through a maximum whose value and location (the latter is located in the lower quarter of the left wall) varies with the inclination, then decreases with y to reach its minimum in the upper corner on the cavity. The effect of the inclination is important only in the lower part of the left wall (y < 0.28); in this region the inclination 60° is the least favorable to the mass transfer. By applying a heat generation with an intensity corresponding to $R = 80$, we can observe strong changes in the shape of Sh_1(y) curves. In fact, Sh_1(y) is seen to go first through a relative maximum followed by a minimum then increases afterward with y to reach another relative maximum located in the immediate vicinity of the upper corner of the cavity. The region where the inclination effect is very remarkable becomes larger than in the case of $R = 0$ (it nearly covers the lower quarter of the heated wall). In most of this region, the inclination 60° becomes the most favorable to mass transfer (instead of 0° in the case of $R = 0$). For $R = 80$, the local minimum of mass transfer is located in the vicinity of y = 0.5 for all the inclinations considered. The maximum of mass transfer is located near the upper corner for γ = 0° and 30°, while it is located in the lower quarter of the left wall for γ = 60°. A close inspection of the streamlines show that the center of the main cell (see that it is located in the lower part of the cavity) is closer to the left wall in the case of the inclination 60° compared to 0° and 30°. This fact, combined with the relatively weak intensity of the secondary cell, explains why the maximum of Sh_1(y) is located in the lower part of the left wall. For γ = 0° and 30°, the conditions are favorable for the secondary cell which affects more the mass transfer on the left wall (larger intensity for the secondary cell and weaker effect of the main cell on the transfer from the lower part of the left wall). Therefore, this cell, which is counter-clockwise rotating, interacts first with the upper part of the left wall and favors mass transfer there, which leads to the creation of a maximum of Sherwood number in the upper part of the left wall. By examining the evolution of Sh_0(y) on the cold wall in Fig. 9b, we can understand easily that the strong changes exhibited by Sh_1(y) when R goes from 0 to 80 are mainly due to the birth of the secondary flow cell. In fact, for both $R = 0$ and 80, the mass transfer across the right wall is governed by a main cell. As a result, the curves of Sh_0(y) globally maintain their qualitative behavior when R increases from 0 to 80. The change of the intensity of the main cell and the change of the distribution of the velocities inside the latter are responsible for the change of the slope of the curves and the position and the depth of the minimum observed for $Sh_0(y)$. For $Sr = -0.5$, the most important changes are observed in the case of $R = 80$. For the left wall, Fig. 9c shows that the transport of mass by thermodiffusion destroys the relative maximum observed for $Sh_1(y)$ in the lower part of the left wall. Furthermore, it attenuates strongly the variation exhibited by $Sh_1(y)$ in the case of $\gamma = 60°$ (the latter is nearly constant in the central portion of the left wall). Also, the local Sherwood number on the right wall is strongly affected by the thermodiffusion in the case of $R = 80$ as it can be seen from Fig. 9d. In comparison with the case of $Sr = 0$, the thermodiffusion intensifies/attenuates the mass transfer (compare the absolute values) around the position y = 0.25/(y = 1.75), which creates new extrema in the curves of $Sh_0(y)$ (a maximum in the upper part and a new minimum in the lower part). Note that the important attenuation exhibited by the mass transfer around y = 1.75 is even accompanied by a change of the sign for Sherwood in the case of the inclinations 0° and 30°. This means that the temperature gradient around this position is so important that thermodiffusion mass flux overcomes the mass flux induced by the concentration gradient.

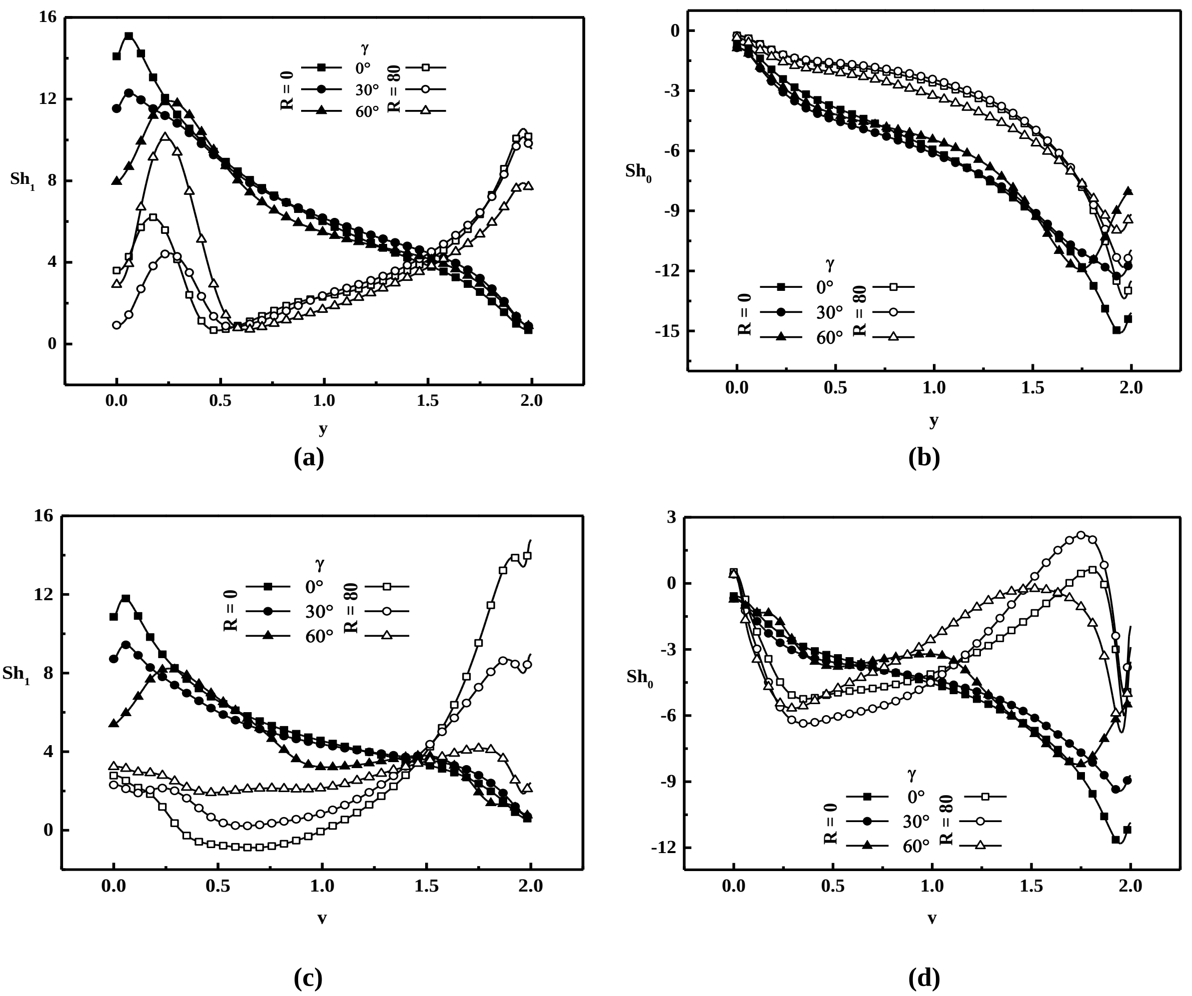

Figure 9: Local Sherwood number in the heated (a, c) and cooled (b, d) walls for; $\mathrm{Sr} = 0$ (a, b) and -0.5 (c, d) and various γ.

Conclusion

Thermosolutal natural convection in a rectangular cavity having an aspect ratio A = 2 has been studied numerically in the presence of Soret effect and internal heat generation. Short adiabatic and impermeable walls and long walls heated and salted with constant but different temperatures and concentrations formed the cavity. The numerical study was based on hybrid lattice-Boltzmann finite-difference method. The Rayleigh number ratio was from 0 to 80, inclination angle from 0° to 60° and Soret parameter Sr = 0 and -0.5, the remaining other parameters were maintained constant. Based on the findings, fluid flow, heat, and mass transfer characteristics are influenced by the three parameters but their effects are more or less important. The monocellular nature of the flow, obtained for $R =$

0 is not destroyed by varying the cavity inclination and the Soret parameter, even though the latter two parameters have a limited qualitative effect and a significant quantitative effect. The monocellular structure is rather destroyed by the increase of the parameter R. The Soret parameter and the cavity inclination do not affect the trend of variation of the mean temperature vs. R; their effects become perceptible at high values of this parameter. In addition, the inclination $\gamma = 60°$ leads to high mean temperatures compared to the other inclinations. The effect of R on mean concentration is amplified in the presence of Soret effect but limited in the absence of Soret effect. This study shows also that negative Soret parameter combined with high internal heat generation and a relatively high inclination is important when the objective is to maintain the fluid at a high concentration of species (the species concentration may be multiplied by more than 2 when R passes from 0 to 80). For $R = 0$ the most important local heat transfer occurs on the upper/lower part of the cold /hot wall. For $R = 80$, the presence of bicellular flow combined with the important elevation undergone by the fluid temperature, makes both the cold and hot walls playing a cooling role with the most important exchanges taking place at the upper part of these walls. The effect of inclination is seen to be important on the local heat transfer; there are situations where the local Nusselt number is multiplied by a factor of 2 by varying γ in the range from 0° to 60°. High internal generation and/or the thermodiffusion leads to comlex behavior for the local Sherwood number. At $R = 80$ and, depending on the inclination, the thermoodiffusion mass flux may overcome the transport of mass induced by concentration gradient, and thereby creates an inwards movement of species through the least concentrated wall.

Nomenclature

A	Aspect ratio of the cavity
g	Acceleration due to gravity, *m/s^2*
H	Height of the square cavity, *m*
Ra_E	External Rayleigh number
Nu	Local Nusselt number
Pr	Prandtl number
T	Temperature, *K*
ΔT	Temperature difference, *K*
T_1	Temperature of the left wall, *K*
T_0	Temperature of the right wall, *K*
u	x component of velocity
v	y component of velocity
f	Vector of distribution functions
c	Discrete velocity of the particle located at r
Δt	Time step
F_y	Buoyancy force

Greek symbols

ψ	Stream function
β	Volume expansion coefficient, *K^{-1}*
θ	Dimensionless temperature
ϕ	Dimensionless concentration
Ω	Dimensionless vorticity

References

[1] Y. Kamotani, L.W. Wang, S. Ostrach, H.D. Jiang, Experimental study of natural convection in shallow enclosures with horizontal temperature and concentration gradients, *Int. J. Heat Mass Transfer*, Volume 28, Pages 165–173, 1985.
[2] H. Han, T.H. Kuehn, Double diffusive natural convection in a vertical rectangular enclosure i: experimental study, *Int. J. Heat Mass Transfer*, Volume 34, Pages 449–459, 1991.
[3] H. Han, T.H. Kuehn, Double diffusive natural convection in a vertical rectangular enclosure ii: numerical study, *Int. J. Heat Mass Transfer,* Volume 34, Pages 461–471, 1991.
[4] F. Alavyoon, On natural convection in vertical porous enclosures due to prescribed fluxes of heat and mass at the vertical boundaries, *Int. J. Heat Mass Transfer,* Volume 25, Pages 2479-2498, 1993.
[5] A. Amahmid, M. Hasnaoui and P. Vasseur, Etude analytique et numérique de la convection naturelle dans une couche poreuse de Brinkman doublement diffusive, *Int. J. Heat Mass Transfer*, Volume 42, Pages 2991-3005, 1999.
[6] M. Er-Raki, M. Hasnaoui, A. Amahmid and M. Mamou, Soret effect on the boundary layer flow regime in a vertical porous enclosure subject to horizontal heat and mass fluxes, *Int. J. Heat Mass Transfer,* Volume 49, Pages 3111–3120, 2006.
[7] L. Wang, B. Shi, Z. Chai and X. Yang, Regularized lattice Boltzmann model for double-diffusive convection in vertical enclosures with heating and salting from below, *Applied Thermal Engineering*, Volume 103, Pages 365–376, 2016.
[8] O.V. Trevisan, A. Bejan, Mass and heat transfer by high Rayleigh number convection in a porous medium heated from below, *Int. J. Heat Mass Transfer*, Volume 30, Pages 2341–2356, 1987.
[9] M. Mamou, P. Vasseur, M. Hasnaoui, On numerical stability analysis of double-diffusive convection in confined enclosures, *J. Fluid Mech*, Volume 433, Pages 209–250, 2001.

[10] M. Bourich, M. Hasnaoui, A. Amahmid, M. Mamou, Onset of convection and finite amplitude flow due to Soret effect within a horizontal sparsely packed porous enclosure heated from below, *Int. J. Heat Fluid Flow*, Volume 26, Pages 513–525, 2005.
[11] A. Mansour, A. Amahmid, M. Hasnaoui, M. Mamou, Onset of thermosolutal convection in a shallow porous layer heated and salted from below and subject to a horizontal heat flux balanced by a Soret mass flux, *Int. J. Heat Mass Transfer*, Volume 50, Pages 2148–2160, 2007.
[12] J.K. Platten, M.M. Bou-Ali, J.F. Dutrieux, Enhanced molecular separation in inclined thermogravitational columns, *J. Phys. Chem. B*, Volume 107, Pages 11763–11767, 2003.
[13] B. Elhajjar, A. Mojtabi, P. Costesèque, M.C. Charrier-Mojtabi, Separation in an inclined porous thermogravitational cell, *Int. J. Heat Mass Transfer*, Volume 53, Pages 4844–4851, 2010.
[14] A. Rtibi, M. Hasnaoui and A. Amahmid, Analytico-numerical study of optimal separation of species in an inclined Darcy–Brinkman porous cavity saturated with a binary mixture, *Acta Astronautica*, Volume 98, Pages 71–85, 2014.
[15] A. Rtibi, M. Hasnaoui and A. Amahmid, Magnetic field effect on Soret driving free convection in an inclined porous cavity saturated by a conducting binary mixture, *Int. J. Numer. Meth. Heat Fluid Flow*, Volume 24, Pages 1715-1735, 2014.
[16] M. Jourabian, M. Farhadi and A.A. Rabienataj Darzi, Simulation of natural convection melting in an inclined cavity using lattice Boltzmann method, *Scientia Iranica B*, Volume 19, Pages 1066–1073, 2012.
[17] H. F. Oztop, M. Mobedi, E. Abu-Nada and I. Pop, A heatline analysis of natural convection in a square inclined enclosure filled with a CuO nanofluid under non-uniform wall heating condition, *Int. J. Heat Mass Transfer*, Volume 55, Pages 5076–5086 , 2012.
[18] E. Abu-Nada and A. J. Chamkha, Mixed convection flow in a lid-driven inclined square enclosure filled with a nanofluid, *European Journal of Mechanics B/Fluids*, Volume 29, Pages 472–482, 2010.
[19] M. Hati, A. Raji, M. Hasnaoui, M. Naïmi, and M. El Abdallaoui, Optimal natural convection heat transfer improvement by combining periodic heating temperature, cavity inclination, and nanofluid, *Heat Transfer Engineering*, Volume 38, Pages 931-947, 2017.
[20] F.A. Kulacki, M.E. Nagle, Natural convection in horizontal fluid layers with volumetric energy sources, *ASME J. Heat Transfer*, Volume 97, Pages 204–211, 1975.
[21] J.H. Lee, R.J. Goldstein, An experimental study on natural convection in an inclined square enclosure containing internal energy sources, *ASME J. Heat Transfer*, Volume 110, Pages 345–349, 1988.
[22] A.G. Churbanov, P.N. Vabischevich, V.V. Chudanov, V.F. Strizhov, A numerical study on natural convection of a heat-generation fluid in rectangular enclosures, *Int. J. Heat Mass Transfer*, Volume 37, Pages 2969–2984, 1994.
[23] P. Deshmukh, S. K. Mitra and U.N. Gaitonde, Investigation of natural circulation in cavities with uniform heat generation for different Prandtl number fluids, *Int. J. Heat Mass Transfer*, Volume 54, Pages 1465–1474, 2011.
[24] M. A. Teamah, A. F. Elsafty, E. Z. Massoud, Numerical simulation of double-diffusive natural convective flow in an inclined rectangular enclosure in the presence of magnetic field and heat source, *Int. Journal Thermal Sciences*, Volume 52, Pages 161-175, 2012.
[25] Q. Zou and X. He, On pressure and velocity boundary conditions for the Lattice Boltzmann BGK Model, *Phys. Fluids*, Volume 9, Pages 1592–1598, 1997.
[26] X. He and L. S. Luo, Lattice-Boltzmann model for the incompressible Navier–Stokes equation, *J. Stat. Phys.*, Volume 88, Pages 927–944, 1997.
[27] M. El Abdallaoui, M. Hasnaoui, and A. Amahmid, Lattice-Boltzmann modeling of natural convection between a square outer cylinder and an inner isosceles triangular heating body, *Numerical Heat Transfer, Part A*, Volume 66, Pages 1076-1096, 2014.
[28] L. S. Luo, Lattice-Gas Automata and Lattice-Boltzmann Equations for Two-Dimensional Hydrodynamics, PhD. Thesis, Georgia Institute of Technology, 1993.
[29] S. Chapman and T. Cowling, Mathematical Theory of Non-uniform Gases, *3rd ed. Cambridge University Press*, Cambridge, 1970.
[30] P. Lallemand and L.S. Luo, Hybrid Finite-difference thermal Lattice Boltzmann equation, *Int. J. Modern Physics B*, Volume 17, Pages 41-47, 2003.